

# Formation of molecular oxygen in ultracold O + OH reaction

Goulven Quémener, Naduvalath Balakrishnan

*Department of Chemistry, University of Nevada Las Vegas, Las Vegas, NV-89154, USA*

Brian K. Kendrick

*Theoretical Division, Los Alamos National Laboratory, Los Alamos, NM-87545, USA*

(Dated: November 3, 2018)

We discuss the formation of molecular oxygen in ultracold collisions between hydroxyl radicals and atomic oxygen. A time-independent quantum formalism based on hyperspherical coordinates is employed for the calculations. Elastic, inelastic and reactive cross sections as well as the vibrational and rotational populations of the product O<sub>2</sub> molecules are reported. A *J*-shifting approximation is used to compute the rate coefficients. At temperatures  $T = 10 - 100$  mK for which the OH molecules have been cooled and trapped experimentally, the elastic and reactive rate coefficients are of comparable magnitude, while at colder temperatures,  $T < 1$  mK, the formation of molecular oxygen becomes the dominant pathway. The validity of a classical capture model to describe cold collisions of OH and O is also discussed. While very good agreement is found between classical and quantum results at  $T = 0.3$  K, at higher temperatures, the quantum calculations predict a larger rate coefficient than the classical model, in agreement with experimental data for the O + OH reaction. The zero-temperature limiting value of the rate coefficient is predicted to be about  $6 \times 10^{-12}$  cm<sup>3</sup> molecule<sup>-1</sup> s<sup>-1</sup>, a value comparable to that of barrierless alkali-metal atom - dimer systems and about a factor of five larger than that of the tunneling dominated F + H<sub>2</sub> reaction.

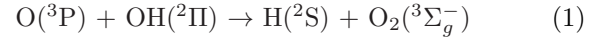
PACS numbers:

## I. INTRODUCTION

Important experimental progress is being made in creating ultracold molecules in tightly bound vibrational levels [1]. Very recently, formation of ground state molecules in the vibrational level  $v = 0$  has been reported by different groups for homonuclear molecules such as Cs<sub>2</sub> [2], Rb<sub>2</sub> [3], as well as for heteronuclear polar molecules such as RbCs [4], KRb [5], and LiCs [7]. There has also been much progress in the measurement of rate coefficients of barrierless reactions involving alkali-metal atoms at cold and ultracold temperatures. This includes atom - molecule collisions such as Rb + Rb<sub>2</sub> [8, 9], Cs + Cs<sub>2</sub> [10, 11], Na + Na<sub>2</sub> [12], Rb/Cs + RbCs [13], and molecule - molecule collisions such as Cs<sub>2</sub> + Cs<sub>2</sub> [10, 14], Na<sub>2</sub> + Na<sub>2</sub> [12], and Rb<sub>2</sub> + Rb<sub>2</sub> [9]. The typical rate coefficients of these reactions are on the order of  $10^{-11} - 10^{-10}$  cm<sup>3</sup> molecule<sup>-1</sup> s<sup>-1</sup> depending on the collisional system, the temperature and the vibrational levels probed. All these experimental studies indicate that inelastic and reactive processes occur at significant rates at ultracold temperatures, in accordance with theoretical predictions on barrier reactions [15, 16, 17, 18, 19, 20] as well as a number of alkali-metal atom - dimer systems [21, 22, 23, 24, 25, 26, 27, 28, 29, 30] such as Li + Li<sub>2</sub>, Na + Na<sub>2</sub> and K + K<sub>2</sub> which proceeds without an energy barrier in the entrance channel. The alkali-metal systems are characterized by triatomic complexes with deep potential wells which make them challenging systems for accurate quantum calculations. For these heavy systems, the density of triatomic states is large and it leads to strong couplings between them, enhancing inelastic quenching or reactive scattering [31]. However,

explicit quantum calculations of molecule - molecule systems involving alkali-metal atoms are computationally intractable. In a recent theoretical study of vibrational relaxation in collisions between H<sub>2</sub> molecules, Quémener et al. [32] showed that the relaxation rate coefficients at ultralow temperature can attain large values for some near-resonant processes which involve simultaneous conservation of internal energy and total internal rotational angular momentum of the colliding molecules.

While there have been a number of theoretical studies of ultracold reactive collisions of tunneling dominated reactions with chemically distinct reactants and products [15, 16, 17, 18, 19, 20], there have been no such studies involving barrierless chemical reactions at ultracold temperatures. Here we investigate the exothermic reaction



at cold and ultracold temperatures as an example of a barrierless chemical reaction involving non-alkali-metal atom systems. The reaction is of key interest in oxygen chemistry in the interstellar medium, OH chemistry in the upper stratosphere and mesosphere, and combustion chemistry (see Ref. [33] and references therein). The OH radical has also been cooled and trapped using the buffer gas and stark decelerator techniques [34, 35, 36, 37]. High precision measurements of its radiative lifetime [38] and its hyperfine constant [39, 40] have recently been reported. An experimental study of scattering between cold OH molecules and He atoms and D<sub>2</sub> molecules has recently been reported [41]. The cooling and trapping studies have stimulated a number of theoretical investigations involving the OH molecule in the last few years.

González-Sánchez et al. [42] reported rotational relaxation and spin-flipping of OH in He collisions at ultralow energies. They found that rotational relaxation occurs more efficiently than elastic collisions at vanishing collision energies. By carrying out quantum calculations of Rb + OH collisions at ultracold temperatures Lara et al. [43, 44] explored the possibility of sympathetic cooling of OH molecules by collisions with Rb atoms. They argued that efficient sympathetic cooling of OH molecules in the ground vibrational state by collisions with Rb atoms is unlikely to occur due to the large inelastic rate coefficient. External fields can also have important effects on ultracold molecular collisions [45, 46, 47]. Avdeenkov and Bohn investigated the effect of external fields on ultracold collisions between OH or OD molecules [48, 49, 50]. Ticknor and Bohn [51] also studied OH–OH collisions in the presence of a magnetic field. They showed that magnetic fields of several thousand Gauss suppress inelastic collision rates by about two orders of magnitude. In a recent study [33], we reported quantum dynamics calculations of reaction (1) for  $T = 10 - 600$  K and found no significant decrease of the rate coefficient in the temperature range 39–10 K, in accordance with conclusions of a recent experimental study by Carty et al. [52]. Our calculations for reaction probabilities were in excellent agreement with those of Xu et al. [53] for collision energies  $E_c > 0.012$  eV.

In this paper, we present the quantum dynamics of reaction (1) at low and ultralow collision energies to explore the behavior of complex forming chemical reactions at cold and ultracold temperatures. Since OH molecules have been experimentally cooled and trapped at low temperatures, we believe that collisional properties of the O + OH reaction will be of considerable interest to the cooling and trapping community. The paper is organized as follows: The details of the quantum mechanical formalism along with convergence tests are discussed in Section II. Results of cross sections, rate coefficients, and state-to-state product distributions are given in Section III. We also include in this section a discussion on the usefulness of a classical model in describing cold collisions of O and OH. Conclusions are presented in Section IV.

## II. METHODOLOGY

### A. Potential energy surfaces

We employed a modified version of the electronically adiabatic ground state ( $1^2A''$ ) potential energy surface (PES) of HO<sub>2</sub> calculated by Kendrick and Pack [55] using a diatomics-in-molecule (DIM) formalism. This new version includes improvements to the long-range behavior and is referred to as the DIMKP PES. In particular, a switching function was implemented which more smoothly “turns-on” the long-range van der Waals potentials for the electronic ground states of both O<sub>2</sub> and OH. This switching function is given by  $f_{\text{switch}} =$

$0.5(\tanh(\alpha(r - r_0)) + 1)$  where  $\alpha = 1$ ,  $r_0 = 7.0 a_0$  for O<sub>2</sub>( $^3\Sigma_g^-$ ) and  $r_0 = 10 a_0$  for OH( $^2\Pi$ ). A minor global refitting of the DIM HO<sub>2</sub> PES to the original set of *ab initio* data was required in order to account for the new switching functions and ensure a smooth transition to the long-range behavior. The same long-range coefficients were used as in the original version of the surface, for OH( $^2\Pi$ ):  $C_6^{\text{O-H}} = 9.295 E_h a_0^6$ ,  $C_8^{\text{O-H}} = 169.09 E_h a_0^8$ ,  $C_{10}^{\text{O-H}} = 4060.85 E_h a_0^{10}$ , and for O<sub>2</sub>( $^3\Sigma_g^-$ ):  $C_6^{\text{O-O}} = 14.89 E_h a_0^6$ ,  $C_8^{\text{O-O}} = 206.67 E_h a_0^8$ , and  $C_{10}^{\text{O-O}} = 3753.745 E_h a_0^{10}$  [55]. The global fit in the interaction region is essentially identical to the original fit with nearly the same rms deviation of 0.099 eV (2.3 kcal/mol). The improvements to the long-range behavior are important for the ultracold collisions studied in this work but should not significantly affect the results of previous scattering calculations at higher (thermal) energies [56]. We present in Fig. 1 the potential energy curves for the 3 lowest  $^2A''$  states of HO<sub>2</sub> for the DIMKP PES, for a O–HO linear approach. We also note in the inset of Fig. 1 that the DIMKP PES predicts a shallow conical intersection along the O–HO approach due to the crossing of the OH( $^2\Pi$ ) and OH( $^4\Sigma$ ) states. For a fixed  $r_{\text{OH}} = 1.83 a_0$ , this crossing occurs at  $R_{\text{O-HO}} = 10.8235 a_0$  and its energy lies  $8.30 \times 10^{-4}$  eV ( $\approx 9.6$  K) below the asymptotic energy of the O + OH channel. For comparison purposes, we also employed the *ab initio* PES computed by Xu, Xie, Zhang, Lin, and Guo [57, 58], referred to as the XXZLG PES. The XXZLG PES has been used in a number of quantum dynamics calculations of the O + OH system at high collision energies [53, 54, 59]. The present DIMKP PES was employed for the first time for this reaction in our previous work [33] and it is preferred at low energies as it includes accurate long-range coefficients.

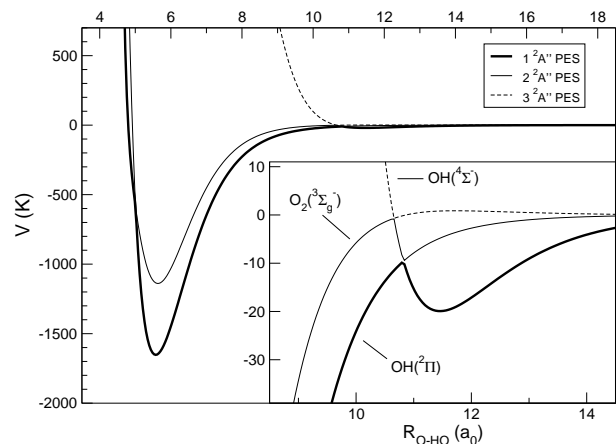


FIG. 1: Potential energy curves for the 3 lowest  $^2A''$  states of HO<sub>2</sub> for the DIMKP PES, for a O–HO linear approach with  $r_{\text{OH}} = 1.83 a_0$ . The conical intersections arising at  $R_{\text{O-HO}} \approx 10.8 a_0$  is shown in the inset.

## B. Quantum mechanical approach and convergence tests

The quantum dynamics calculations have been performed using the adiabatically adjusting principle-axis hyperspherical (APH) approach of Pack and Parker [60]. The method uses the democratic Smith-Whitten hyperspherical coordinates in the inner region ( $\rho < 17 a_0$ ) that includes the triatomic well of the  $\text{HO}_2$  system and the Delves–Fock hyperspherical coordinates in the outer region ( $\rho > 17 a_0$ ) in the valleys of the  $\text{H} + \text{O}_2$  and  $\text{O} + \text{OH}$  arrangement channels. For a given value of the total angular momentum quantum number,  $J$ , and hyperspherical radius,  $\rho$ , the wavefunction is expanded onto a basis set of adiabatic functions, which are eigenfunctions of a triatomic hyperangular Hamiltonian. A hybrid DVR/FBR primitive basis set [61] combined with an Implicit Restarted Lanczos algorithm is used to diagonalize the hyperangular Hamiltonian matrix. The time-independent Schrödinger equation yields a set of differential close-coupling equations in  $\rho$ , which are solved using the log-derivative matrix propagation method of Johnson [62]. The log-derivative matrix is propagated to a matching distance ( $\rho_m$ ) where asymptotic boundary conditions are applied to evaluate the reactance matrix  $K^J$  and the scattering matrix  $S^J$ . The square elements of the  $S^J$  matrix provide the state-to-state transition probabilities,  $P^J$ . The matching distance and all other parameters employed in the calculations were determined by optimization and extensive convergence studies. To secure convergence of the reaction probabilities, the number of hyperspherical channels,  $n$ , included in the close coupling equations is 393. This is sufficient to obtain converged results at low and ultralow energies. The cross sections are calculated using the standard formulae:

$$\sigma_{\text{el}}^J = \frac{\pi}{k^2} |1 - S_{ii}^J|^2 \quad \sigma_{\text{re}}^J = \frac{\pi}{k^2} \sum_{\text{reactive } j} |S_{ij}^J|^2,$$

where  $i, j$  denote initial and final quantum states. The non-thermal elastic and reactive rate coefficients are given by  $\sigma_{\text{el}} \times \nu$  and  $\sigma_{\text{re}} \times \nu$  where  $\nu = \hbar k / \mu$  is the incident velocity for relative motion of the O atom and the OH molecule.

The convergence of the elastic cross section  $\sigma_{\text{el}}^{J=0}$  and the non-thermal reactive rate coefficient  $\sigma_{\text{re}}^{J=0} \times \nu$  are presented in Tab. I and Tab. II for  $\text{O} + \text{OH}(v=0, j=0)$  on the DIMKP PES. At vanishing collision energies, these quantities attain finite values as required by the Bethe–Wigner laws [63, 64]:

$$\sigma_{\text{el}}^{J=0} \rightarrow \text{const.} \quad \sigma_{\text{re}}^{J=0} \times \nu \rightarrow \text{const.}$$

The tables also show convergence of the results with the matching distances. At low energies the elastic cross section converges less rapidly with the matching distance  $\rho_m$  than the reactive one. This is because the long-range contribution to the interaction potential is not negligible compared to the kinetic energy in the entrance channel, even for moderately large values of the hyperradius.

$\rho_m (a_0)$	26.8	32.7	39.9	44.0
$E_c \text{ (eV)}$	$\sigma_{\text{el}}^{J=0}$			
$10^{-10}$	0.4995	0.5019	0.4786	0.4679
$10^{-9}$	0.4965	0.4977	0.4742	0.4635
$10^{-8}$	0.4877	0.4853	0.4610	0.4505
$10^{-7}$	0.4596	0.4472	0.4206	0.4110
$10^{-6}$	0.3708	0.3369	0.3085	0.3021
$10^{-5}$	0.1432	0.1164	0.1108	0.1123
$10^{-4}$	0.005536	0.005214	0.005300	0.005217
$10^{-3}$	0.001531	0.001516	0.001506	0.001507

TABLE I: Convergence of the elastic cross section  $\sigma_{\text{el}}^{J=0}$  in units of  $10^{-13} \text{ cm}^2$  with the matching distance  $\rho_m$  for  $\text{O} + \text{OH}(v=0, j=0)$  using the DIMKP PES, for  $n=393$ .

$\rho_m (a_0)$	26.8	32.7	39.9	44.0
$E_c \text{ (eV)}$	$\sigma_{\text{re}}^{J=0} \times \nu$			
$10^{-10}$	0.1965	0.2777	0.3123	0.3133
$10^{-9}$	0.1954	0.2755	0.3095	0.3104
$10^{-8}$	0.1920	0.2688	0.3010	0.3018
$10^{-7}$	0.1819	0.2490	0.2760	0.2765
$10^{-6}$	0.1544	0.1979	0.2123	0.2119
$10^{-5}$	0.09835	0.1080	0.1080	0.1073
$10^{-4}$	0.03748	0.03713	0.03724	0.03714
$10^{-3}$	0.008704	0.008745	0.008761	0.008765

TABLE II: Convergence of the non-thermal reactive rate coefficients,  $\sigma_{\text{re}}^{J=0} \times \nu$ , in units of  $10^{-10} \text{ cm}^3 \text{ molecule}^{-1} \text{ s}^{-1}$  with the matching distance  $\rho_m$  for  $\text{O} + \text{OH}(v=0, j=0)$  using the DIMKP PES, for  $n=393$ .

Thus, elastic cross sections are generally more sensitive to the long-range tail of the interaction potential. For the parameters in Tab. I and Tab. II the reactive rate coefficients are converged to within 1% while the elastic cross sections are converged within 3%. All of the final results presented here are obtained using  $\rho_m = 44.0 a_0$ , which is especially necessary to get converged results at  $E_c < 10^{-4} \text{ eV}$  [65].

## III. RESULTS AND DISCUSSION

### A. Cross sections and rate coefficients

The  $J=0$  elastic and reactive cross sections are plotted as a function of the collision energy in Fig. 2 for the DIMKP PES. The corresponding non-thermal rate coefficients are presented in Fig. 3. In both figures, the Bethe–Wigner laws are satisfied at ultralow collision energies. The elastic cross section and the reactive rate coefficient converge to values of  $4.6 \times 10^{-14} \text{ cm}^2 \text{ molecule}^{-1}$  and  $3.1 \times 10^{-11} \text{ cm}^3 \text{ molecule}^{-1} \text{ s}^{-1}$  respectively in the

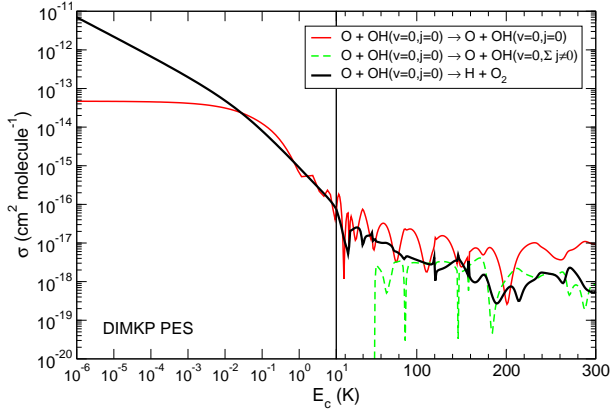


FIG. 2: (Color online)  $J = 0$  cross section as a function of the collision energy for the elastic (red curve), inelastic (green dashed curve) and reactive (black curve) collisions of O atoms with  $\text{OH}(v=0, j=0)$  molecules for the DIMKP PES.

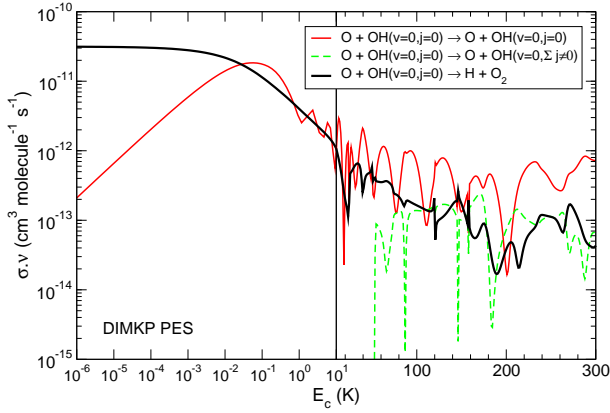


FIG. 3: (Color online)  $J = 0$  non-thermal rate coefficient as a function of the collision energy for the elastic (red curve), inelastic (green dashed curve) and reactive (black curve) collisions of O atoms with  $\text{OH}(v=0, j=0)$  molecules for the DIMKP PES.

limit of zero energy. The elastic rate coefficient and the reactive cross section behave respectively as the square root and the inverse of the square root of the collision energy. The Bethe-Wigner regime is reached at  $E_c \approx 10^{-4}$  K, where the reactive rate coefficient is of about one order of magnitude higher than that of the elastic counterpart. At  $E_c = 10^{-6}$  K the reactive rate coefficient is two orders of magnitude larger than the elastic one. This is reminiscent of other exothermic barrierless systems such as alkali-metal atom - diatom collisions [21, 22, 23, 24, 25, 26, 27, 28, 29]. At energies between  $E_c = 0.01$  K and 30 K, elastic and reactive rate coefficients are of comparable magnitude. For  $E_c > 30$  K, the elastic scattering is more efficient than reactive scattering. The inelastic rotational excitation to the  $j = 1$  level opens up at  $E_c = 52$  K and its cross section is comparable to the reactive contribution.

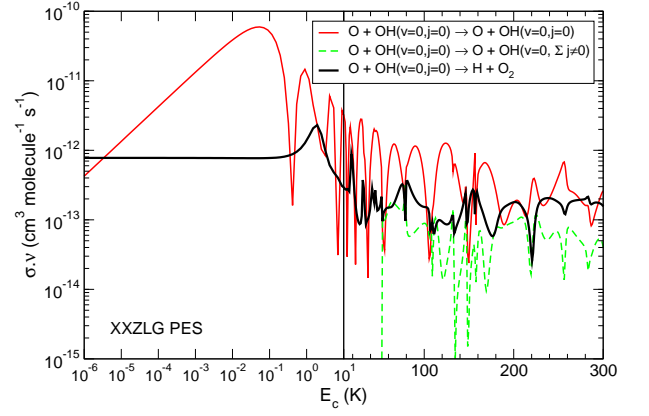


FIG. 4: (Color online) Same as Fig. 3 but for the XXZLG PES.

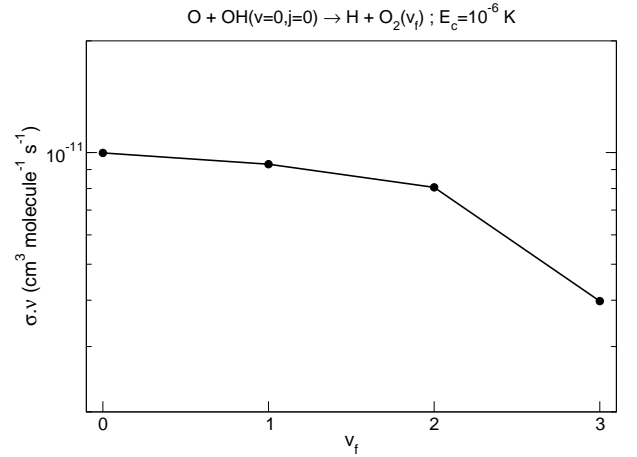


FIG. 5: Vibrational populations of the product  $\text{O}_2$  molecule in  $\text{O} + \text{OH}(v=0, j=0) \rightarrow \text{H} + \text{O}_2(v_f)$  reaction evaluated using the DIMKP PES at a collision energy of  $10^{-6}$  K and  $J = 0$ .

The  $J = 0$  contribution to the elastic, inelastic and reactive rate coefficients evaluated using the XXZLG PES are presented in Fig. 4 as functions of the collision energy. For  $E_c > 1$  K, all three rate coefficients are of comparable magnitudes with those obtained from the DIMKP PES. For  $E_c < 1$  K, the reactive rate coefficient is about two orders of magnitude smaller than that obtained using the DIMKP PES. The differences can be traced to the incomplete description of the long-range interaction potential in the XXZLG PES. It does not properly include the long-range potential in the  $\text{O} + \text{OH}$  channel as it was not designed for quantum dynamics calculations at ultralow energies. Thus, the comparison of the results obtained using the two surfaces highlights the crucial role of the long-range interaction potential in chemical reaction dynamics at low temperatures. The importance of the long-range intermolecular forces in the  $\text{O}-\text{OH}$  system in determining its rate coefficient has been pointed out

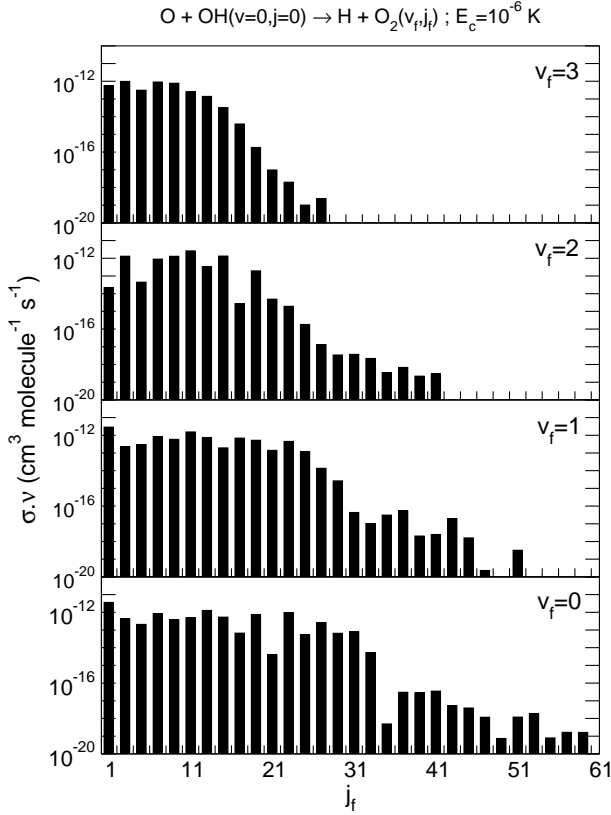


FIG. 6: Rotational populations of the product  $O_2$  molecule in  $O + OH(v=0, j=0) \rightarrow H + O_2(v_f=0, 1, 2, 3, j_f)$  reaction evaluated using the DIMKP PES at a collision energy of  $10^{-6}$  K and  $J=0$ .

by Clary and Werner [66]. In the following, we restrict our calculations to the DIMKP PES.

The vibrational populations of molecular oxygen formed in  $O + OH(v=0, j=0)$  collisions, evaluated using the DIMKP PES at an energy of  $10^{-6}$  K and  $J=0$  are presented in Fig. 5. Oxygen molecules are predominantly formed in vibrational levels  $v_f = [0-2]$  with a slight preference for the ground vibrational state  $v_f=0$ . Thus, a significant fraction of the  $O_2$  molecules formed is in excited vibrational states. The rotational level distributions of molecular oxygen formed in  $O + OH(v=0, j=0)$  collisions for  $J=0$  are presented in Fig. 6 for each final vibrational level  $v_f$  populated by the reaction at an energy of  $10^{-6}$  K. The results show that low rotational levels are generally preferred for each of the final vibrational levels. Since the incident channel includes only the  $s$ -wave, the final rotational distribution is largely determined by the anisotropy of the interaction potential.

Explicit calculations of rate coefficients would require reaction probabilities for all contributing values of the total angular momentum quantum number ( $J$ ). This is a computationally demanding problem for the  $O + OH$  reaction if full quantum dynamics calculations are em-

ployed, especially when many  $J$  values contribute to the reaction probability. The  $J$ -shifting approximation [67] is widely used to compute rate coefficients when full quantum calculations are not practical. This is a good approximation for barrier reactions which involve a transition state but not for complex forming reactions. Nevertheless, the  $J$ -shifting approximation has been applied to the  $O + OH$  reaction in a number of previous studies [33, 53, 68, 69, 70] and it has been demonstrated that it can predict rate coefficients within about 40% of numerically exact calculations [54]. Here we use the  $J$ -shifting approximation [67] to compute the rate coefficients for the  $O + OH$  reaction. The rate coefficient is given by the expression:

$$k_{v,j}(T) = \frac{1}{2\pi\hbar Q_R} \times \left( \sum_J (2J+1) e^{-E_{\text{shift}}^J/(k_B T)} \right) \times \int_0^\infty P_{v,j}^{\text{re}, J=0}(E_c) e^{-E_c/(k_B T)} dE_c \quad (2)$$

where  $k_B$  is the Boltzmann constant,  $P_{v,j}^{\text{re}, J=0}$  is the  $J=0$  reaction probability and  $E_{\text{shift}}^J$  is the height of the effective barrier for a given partial wave  $J$  in the entrance channel. To determine the barrier height for a given partial wave, we first evaluate the effective potential,  $V_{\text{eff}}^J$ :

$$V_{\text{eff}}^J = \frac{\hbar^2 J(J+1)}{2\mu(R_{O-OH})^2} + V_{\text{min}}(R_{O-OH}) \quad (3)$$

where  $V_{\text{min}}(R_{O-OH})$  is the minimum energy path of the reaction as a function of the atom - molecule center-of-mass separation,  $R_{O-OH}$ , and  $\mu$  is the reduced mass of the  $O-OH$  system. In Eq. (2),  $Q_R = Q_{\text{trans}} \times Q_{\text{el}}$  is the reactant partition function. For the translational partition function we used the standard formula,  $Q_{\text{trans}} = \left( \frac{\mu k_B T}{2\pi\hbar^2} \right)^{3/2}$ . For the electronic partition function we used the expression given by Graff and Wagner [71]:

$$Q_{\text{el}} = \frac{(5 + 3e^{-228/T} + e^{-326/T})(2 + 2e^{-205/T})}{2}.$$

The effective barriers,  $V_{\text{eff}}^J$ , for the DIMKP PES are shown in Fig. 7 for  $J = [0-200; 10]$ . As Fig. 7 illustrates, the “reef” visible in the effective potential at  $R_{O-OH} = 5 a_0$  for low values of  $J$  becomes an effective barrier for  $J \geq 70$  as indicated by the bold line. The barrier heights  $E_{\text{shift}}^J$  and their locations  $R_{\text{shift}}^J$  are reported in table III for  $J = [1-10]$ .

The elastic, inelastic, and reactive rate coefficients of the  $O + OH(v=0, j=0)$  reaction evaluated using the  $J$ -shifting method for the DIMKP PES are shown in Fig. 8 for  $T = 10^{-6} - 10^3$  K. As indicated earlier, the Bethe-Wigner regime is reached for temperatures below  $T \approx E_c \approx 10^{-4}$  K. The value of the rate coefficient in the zero-energy limit is  $6.2 \times 10^{-12} \text{ cm}^3 \text{ molecule}^{-1} \text{ s}^{-1}$ . This is a factor of 5 smaller than the rate coefficient reported as  $\sigma_{\text{re}}^{J=0} \times \nu$  in Fig. 3. The difference comes



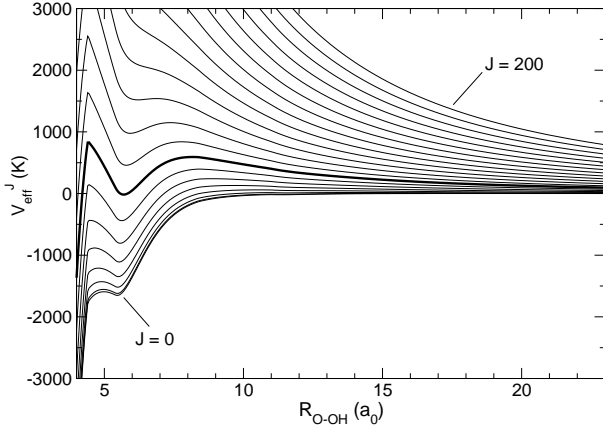


FIG. 7: Effective potentials  $V_{\text{eff}}^J$  as functions of  $R_{\text{O-OH}}$  for  $J = [0 - 200; 10]$  for the DIMKP PES. The bold line corresponds to  $J = 70$ .

from the electronic partition function in the denominator in Eq. 2, which is equal to 5 as  $T \rightarrow 0$ . In experiments using the stark decelerator methods, OH molecules were cooled to  $T = 10 - 100$  mK. In this temperature range, our computed values of the elastic rate coefficients are comparable to the reactive ones and will not favor sympathetic cooling of OH by collisions with O atoms. Similar conclusions have been found by Lara et al. [43, 44] for collisions between OH molecules with Rb atoms. The relatively large rate coefficient for the reaction in the zero-temperature limit indicates that barrierless exothermic reactions occur at significant rates at ultracold temperatures, in agreement with similar results for alkali-metal atom - diatom reactions [21, 22, 23, 24, 25, 26, 27, 28, 29]. Fig. 8 shows that the minimum value of the rate coefficient for the O + OH reaction is about  $4.9 \times 10^{-12} \text{ cm}^3 \text{ molecule}^{-1} \text{ s}^{-1}$  at  $T = 5 \times 10^{-3}$  K. This provides a lower limit for O<sub>2</sub> formation by reaction (1). We note that the inelastic process becomes more probable than the reactive process for  $T > 330$  K.

### B. Classical capture model

We shall now compare our quantum dynamics results with a classical capture model also known as the Langevin model [72]. This model has been shown to work quite well for a certain range of collision energy, for atom-exchange reactions such as K + K<sub>2</sub> [23], Li + Li<sub>2</sub> [24], and also for non-reactive Rb + OH collisions [43, 44]. We have shown [31] that the Langevin model predicts rate coefficients in close agreement with experimental values for Rb + Rb<sub>2</sub> [8], Cs + Cs<sub>2</sub> [10, 11], and Rb/Cs + RbCs [13] collisions reported recently. For the O + OH reaction, Clary and Werner [66] used an adiabatic capture theory [73], while Davidsson and Nyman [74] used a generalized Langevin model. Both studies showed good

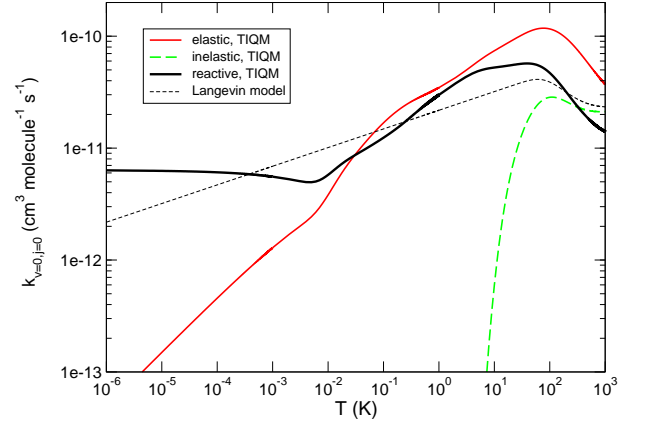


FIG. 8: (Color online) Rate coefficients of O + OH ( $v = 0, j = 0$ ) for the elastic (red curve), inelastic (green dashed curve) and reactive (black curve) collisions for the DIMKP PES. The rate coefficient from a classical Langevin model (black dashed curve) is also shown (see text for detail).

agreement between theoretical and experimental rate coefficients. Here we test the validity of the Langevin model against a TIQM and  $J$ -shifting method for the O + OH reaction. For a non-rotating diatomic molecule ( $j = 0$ ) at large atom - molecule separations  $R_{\text{O-OH}}$ , for a given value of  $J$ , the interaction potential can be approximated by an effective potential,  $V_{\text{Lang}}^J$ , composed of a repulsive centrifugal term and an attractive van der Waals term:

$$V_{\text{Lang}}^J = -\frac{\hbar^2 J(J+1)}{2\mu(R_{\text{O-OH}})^2} - \frac{C_6^{\text{O-OH}}}{(R_{\text{O-OH}})^6}.$$

At an atom - diatom distance of

$$R_{\text{Lang}}^J = \left( \frac{6\mu C_6^{\text{O-OH}}}{\hbar^2 J(J+1)} \right)^{1/4},$$

the height of the effective potential is given by:

$$E_{\text{Lang}}^J = \frac{2}{3\sqrt{3}} (C_6^{\text{O-OH}})^{-1/2} \left( \frac{\hbar^2 J(J+1)}{2\mu} \right)^{3/2}.$$

The quantities  $E_{\text{Lang}}^J$  and  $R_{\text{Lang}}^J$  are reported in Tab. III for  $J = 1 - 10$ . The  $C_6^{\text{O-OH}}$  coefficient is evaluated by fitting the long-range part of the minimum energy path  $V_{\text{min}}(R_{\text{O-OH}})$ . This yielded a value of  $C_6^{\text{O-OH}} \approx 9.2 E_h a_0^6$  which is much smaller than the sum of the atom - atom coefficients  $C_6^{\text{O-H}} + C_6^{\text{O-O}} = 24.2 E_h a_0^6$ . In the DIM model, the smaller  $C_6^{\text{O-OH}}$  coefficient is due to the presence of significant diatomic mixing in the OH diatomic states for  $r_{\text{OH}} = 1.83 a_0$  (see for example Eqs. 34 – 37 in Ref. [55]). This mixing gives rise to an effective  $C_6$  coefficient of the O-HO approach of  $\alpha_1 C_6^{\text{O-H}} + \alpha_2 C_6^{\text{O-O}} = 9.2 E_h a_0^6$  where the multiplicative constants  $\alpha_1$  and  $\alpha_2$  depend on the level of diatomic mixing. As  $r_{\text{OH}}$  increases, the diatomic mixing decreases and  $\alpha_1 \rightarrow 1$  and  $\alpha_2 \rightarrow 1$ . The dependence of the long-range coefficients for atom -

diatom interactions on the diatomic separation has also been noted and investigated in recent work on the Li + Li<sub>2</sub> and Na + Na<sub>2</sub> systems [75, 76]. For the atom-molecule reduced mass we used  $\mu = 15023.74$  *au*. In the Langevin model, the rate coefficient as a function of the temperature is given by the expression:

$$k_{\text{Lang}}(T) = \frac{\pi}{Q_{\text{el}}} \left( \frac{8k_B T}{\pi \mu} \right)^{1/2} \left( \frac{2C_6^{\text{O-OH}}}{k_B T} \right)^{1/3} \Gamma(2/3).$$

$J$	$E_{\text{shift}}^J$ (K)	$R_{\text{shift}}^J$ (a <sub>0</sub> )	$E_{\text{Lang}}^J$ (K)	$R_{\text{Lang}}^J$ (a <sub>0</sub> )
1	0.022	25.4	0.022	25.4
2	0.11	19.3	0.11	19.3
3	0.30	18.6	0.32	16.3
4	0.54	18.4	0.68	14.3
5	0.86	18.0	1.26	12.9
6	1.26	17.5	2.08	11.9
7	1.75	17.1	3.20	11.1
8	2.34	16.7	4.68	10.4
9	3.04	16.4	6.53	9.8
10	3.84	16.1	8.83	9.3

TABLE III: Comparison of the heights and positions of the effective barriers between the  $J$ -shifting approximation and the Langevin model.

The rate coefficient predicted by the Langevin model is plotted in Fig. 8 (black dashed curve). Except in the Bethe-Wigner regime for  $T < 10^{-4}$  K, where the classical model is not valid, the Langevin model predicts rate coefficients in semi-quantitative agreement with those obtained from the quantum calculations. Overall, the reactive rate coefficients oscillate slightly around the Langevin line, as in other barrierless systems such as K + K<sub>2</sub> [23] and Li + Li<sub>2</sub> [24]. However, the Langevin model yields good agreement only for a restricted range of temperatures. The lower limit of the model prediction is restricted by the number of partial waves included in the calculations. In previous studies [23, 24], it has been found that when three or more partial waves are included, the quantum and classical results are in good agreement. If less than three partial waves are involved, the quantum character becomes dominant and the results cannot be compared with the classical model. These previous studies have also shown that the maximum of the quenching rate coefficient for a given partial wave  $J$  occurs at about a collision energy comparable to the height of the barrier,  $E_{\text{Lang}}^J$ . Thus, the lower limit corresponds to a collision energy of  $E_{\text{Lang}}^{J=3} = 0.32$  K (see Tab.III) for the present system. The upper limit is bounded by the long-range part of the potential. When the Langevin radius  $R_{\text{Lang}}^J$  is located at a distance where the long-range part of the potential is not described by the van der Waals interaction,  $E_{\text{Lang}}^J$  will differ from  $E_{\text{shift}}^J$ . In this case, the classical results will differ from the quantum calculations. Tab. III

shows that this is the case for  $J = 3$  and the upper limit of the model also corresponds to a collision energy of  $E_{\text{Lang}}^{J=3} = 0.32$  K. Thus, the Langevin model gives quantitative agreement for temperatures around  $T \approx 0.3$  K, as seen in Fig. 8. For  $T > 0.3$  K, the rate coefficient depends on the exact details of the effective potential in the entrance channel. However, the classical result is in overall agreement with the quantum result, though the classical model predicts a smaller value for the rate coefficient. This is because  $E_{\text{shift}}^J < E_{\text{Lang}}^J$  for  $J > 3$  (see Tab. III) and reactivity is less probable to occur with the Langevin model. Therefore, the Langevin model provides a lower limit of the rate coefficients for  $T = 1 - 100$  K which affirms the theoretical conclusions of Ref. [33] and experimental conclusions of Ref. [52], that the rate coefficient of reaction (1) is unlikely to vanish for  $T < 10$  K. We also note that the Langevin rate coefficient is in semi-quantitative agreement with the inelastic rate coefficient in the range  $T = 100 - 1000$  K. The difference is less than 30 %.

#### IV. CONCLUSION

This paper presents the first quantum mechanical investigation of an ultracold barrierless reaction with chemically distinct reactants and products. We investigated dynamics of molecular oxygen formation in ultracold collisions of the hydroxyl radical and atomic oxygen using a time-independent quantum mechanical method based on hyperspherical coordinates. It has been found that formation of molecular oxygen occurs with a relatively large rate coefficient of  $6.2 \times 10^{-12}$  cm<sup>3</sup> molecule<sup>-1</sup> s<sup>-1</sup> at ultracold temperatures. The oxygen molecules are mainly formed in the  $v = 0 - 2$  vibrational levels with a slight preference for the  $v = 0$  level. Calculations show that at temperatures of  $T = 10 - 100$  mK, the elastic cross sections are not large enough to achieve efficient evaporative cooling in collisions between OH molecules and O atoms. We predict a lower limit of  $4.9 \times 10^{-12}$  cm<sup>3</sup> molecule<sup>-1</sup> s<sup>-1</sup> for the rate coefficient for the O + OH( $v = 0, j = 0$ ) reaction at  $T = 5 \times 10^{-3}$  K. This shows that formation of O<sub>2</sub> molecules is significant even at ultracold temperatures. It has been found that a classical capture model is valid for temperatures around  $T \approx 0.3$  K where quantum and classical calculations yield comparable results. Based on our analysis of the long-range interaction potential we find that for  $T = 1 - 10$  K the Langevin model can provide a lower limit to the quantum reactive rate coefficients calculated within the  $J$ -shifting approximation.

Future work will consider the effects of the geometric phase and non-adiabatic couplings between different PESs of HO<sub>2</sub> on the reaction dynamics. The geometric phase due to the conical intersection of two PESs may have an important effect at low and ultralow collision energies where only a few partial waves contribute to the reaction probabilities.

## V. ACKNOWLEDGMENTS

This work was supported by NSF grants #PHY-0555565 (N.B.) and #ATM-0635715 (N.B.). B.K.K. acknowledges that part of this work was done under the auspices of the US Department of Energy at Los

Alamos National Laboratory. Los Alamos National Laboratory is operated by Los Alamos National Security, LLC, for the National Nuclear Security Administration of the US Department of Energy under contract DE-AC52-06NA25396.

- 
- [1] P. L. Gould, *Science* **322**, 203 (2008).
  - [2] M. Viteau, A. Chotia, M. Allegrini, N. Bouloufa, O. Dulieu, D. Comparat, and P. Pillet, *Science* **321**, 232 (2008).
  - [3] F. Lang, K. Winkler, C. Strauss, R. Grimm, and J. Hecker Denschlag *Phys. Rev. Lett.* **101**, 133005 (2008).
  - [4] J. M. Sage, S. Sainis, T. Bergeman, and D. DeMille, *Phys. Rev. Lett.* **94**, 203001 (2005).
  - [5] K.-K. Ni, S. Ospelkaus, M. H. G. de Miranda, A. Pe'er, B. Neyenhuis, J. J. Zirbel, S. Kotochigova, P. S. Julienne, D. S. Jin, and J. Ye, *Science* **322**, 231 (2008).
  - [6] J. G. Danzl, E. Haller, M. Gustavsson, M. J. Mark, R. Hart, N. Bouloufa, O. Dulieu, H. Ritsch, and H.-C. Nägerl, *Science* **321**, 1062 (2008).
  - [7] J. Deiglmayr, A. Grochola, M. Repp, K. Mörtlbauer, C. Glück, J. Lange, O. Dulieu, R. Wester, and M. Weidemüller, *Phys. Rev. Lett.* **101**, 133004 (2008).
  - [8] R. Wynar, R. S. Freeland, D. J. Han, C. Ryu and D. J. Heinzen, *Science* **287**, 1016 (2000).
  - [9] N. Syassen, T. Volz, S. Teichmann, S. Dür, and G. Rempe, *Phys. Rev. A* **74**, 062706 (2006).
  - [10] N. Zahzam, T. Vogt, M. Mudrich, D. Comparat and P. Pillet, *Phys. Rev. Lett.* **96**, 023202 (2006).
  - [11] P. Staunum, S. D. Kraft, J. Lange, R. Wester, and M. Weidemüller, *Phys. Rev. Lett.* **96**, 023201 (2006).
  - [12] T. Mukaiyama, J. R. Abo-Shaer, K. Xu, J. K. Chin, and W. Ketterle, *Phys. Rev. Lett.* **92**, 180402 (2004).
  - [13] E. R. Hudson, N. B. Gilfoy, S. Kotochigova, J. M. Sage, and D. DeMille, *Phys. Rev. Lett.* **100**, 203201 (2008).
  - [14] F. Ferlaino, S. Knoop, M. Mark, M. Berninger, H. Schöbel, H.-C. Nägerl, and R. Grimm, *Phys. Rev. Lett.* **101**, 023201 (2008).
  - [15] N. Balakrishnan and A. Dalgarno, *Chem. Phys. Lett.* **341**, 652 (2001).
  - [16] E. Bodo, F. A. Gianturco, and A. Dalgarno, *J. Chem. Phys.* **116**, 9222 (2002).
  - [17] E. Bodo, F. A. Gianturco, N. Balakrishnan, and A. Dalgarno, *J. Phys. B: At. Mol. Opt. Phys.* **37**, 3641 (2004).
  - [18] P. F. Weck and N. Balakrishnan, *J. Chem. Phys.* **122**, 154309 (2005).
  - [19] P. F. Weck and N. Balakrishnan, *Int. Rev. Phys. Chem.* **25**, 283 (2005).
  - [20] G. Quémener and N. Balakrishnan, *J. Chem. Phys.* **128**, 224304 (2008).
  - [21] P. Soldán, M. T. Cvitaš, J. M. Hutson, P. Honvault, and J.-M. Launay, *Phys. Rev. Lett.* **89**, 153201 (2002).
  - [22] G. Quémener, P. Honvault, and J.-M. Launay, *Eur. Phys. J. D* **30**, 201 (2004).
  - [23] G. Quémener, P. Honvault, J.-M. Launay, P. Soldán, D. E. Potter, and J. M. Hutson, *Phys. Rev. A* **71**, 032722 (2005).
  - [24] M. T. Cvitaš, P. Soldán, J. M. Hutson, P. Honvault, and J.-M. Launay, *Phys. Rev. Lett.* **94**, 033201 (2005).
  - [25] M. T. Cvitaš, P. Soldán, J. M. Hutson, P. Honvault, and J.-M. Launay, *Phys. Rev. Lett.* **94**, 200402 (2005).
  - [26] J. M. Hutson and P. Soldán, *Int. Rev. Phys. Chem.* **25**, 497 (2006).
  - [27] J. M. Hutson and P. Soldán, *Int. Rev. Phys. Chem.* **26**, 1 (2007).
  - [28] G. Quémener, J.-M. Launay, and P. Honvault, *Phys. Rev. A* **75**, 050701(R) (2007).
  - [29] M. T. Cvitaš, P. Soldán, J. M. Hutson, P. Honvault, and J.-M. Launay, *J. Chem. Phys.* **127**, 074302 (2007).
  - [30] G. Quémener, P. Honvault, J.-M. Launay, *Eur. Phys. J. D* **49**, 75 (2008).
  - [31] G. Quémener, N. Balakrishnan, and A. Dalgarno, in *Cold Molecules: Theory, Experiment, Applications*, R. V. Krems, W. C. Stwalley, and B. Friedrich (Eds.), CRC Press (2009).
  - [32] G. Quémener, N. Balakrishnan, and R. V. Krems, *Phys. Rev. A* **77**, 030704(R) (2008).
  - [33] G. Quémener, N. Balakrishnan, and B. K. Kendrick, arXiv:0810.2832v1 [physics.atom-ph], accepted in *J. Chem. Phys.*
  - [34] J. R. Bochinski, E. R. Hudson, H. J. Lewandowski, G. Meijer, and J. Ye, *Phys. Rev. Lett.* **91**, 243001 (2003).
  - [35] J. R. Bochinski, E. R. Hudson, H. J. Lewandowski, and J. Ye, *Phys. Rev. A* **70**, 043410 (2004).
  - [36] S. Y. T. van de Meerakker, P. H. M. Smeets, N. Vanhaecke, R. T. Jongma, and G. Meijer, *Phys. Rev. Lett.* **94**, 023004 (2005).
  - [37] B. C. Sawyer, B. L. Lev, E. R. Hudson, B. K. Stuhl, M. Lara, J. L. Bohn, and J. Ye, *Phys. Rev. Lett.* **98**, 253002 (2007).
  - [38] S. Y. T. van de Meerakker, N. Vanhaecke, M. P. J. van der Loo, G. C. Groenenboom, and G. Meijer, *Phys. Rev. Lett.* **95**, 013003 (2005).
  - [39] E. R. Hudson, H. J. Lewandowski, B. C. Sawyer, and J. Ye, *Phys. Rev. Lett.* **96**, 143004 (2006).
  - [40] B. L. Lev, E. R. Meyer, E. R. Hudson, B. C. Sawyer, J. L. Bohn, and J. Ye, *Phys. Rev. A* **74**, 061402(R) (2006).
  - [41] B. C. Sawyer, B. K. Stuhl, D. Wang, M. Yeo, and J. Ye, arXiv:0806.2624v1 [physics.atom-ph].
  - [42] L. González-Sánchez, E. Bodo, and F. A. Gianturco, *Phys. Rev. A* **73**, 022703 (2006).
  - [43] M. Lara, J. L. Bohn, D. Potter, P. Soldán and J. M. Hutson, *Phys. Rev. Lett.* **97**, 183201 (2006).
  - [44] M. Lara, J. L. Bohn, D. E. Potter, P. Soldán and J. M. Hutson, *Phys. Rev. A* **75**, 012704 (2007).
  - [45] R. V. Krems, *Int. Rev. Phys. Chem.* **24**, 99 (2005).
  - [46] R. V. Krems, *Phys. Chem. Chem. Phys.* **10**, 4079 (2008).
  - [47] T. V. Tscherbul and R. V. Krems, *J. Chem. Phys.* **129**, 034112 (2008).
  - [48] A. V. Avdeenkov and J. L. Bohn, *Phys. Rev. A* **66**, 052718 (2002).
  - [49] A. V. Avdeenkov and J. L. Bohn, *Phys. Rev. Lett.* **90**,



- 043006 (2003).
- [50] A. V. Avdeenkov and J. L. Bohn, Phys. Rev. A **71**, 022706 (2005).
  - [51] C. Ticknor and J. L. Bohn, Phys. Rev. A **71**, 022709 (2005).
  - [52] D. Carty, A. Goddard, S. P. K. Kohler, I. R. Sims, and I. W. M. Smith, J. Phys. Chem. A **110**, 3101 (2006).
  - [53] C. Xu, D. Xie, P. Honvault, S. Y. Lin, and H. Guo, J. Chem. Phys. **127**, 024304 (2007).
  - [54] S. Y. Lin, H. Guo, P. Honvault, C. Xu, and D. Xie, J. Chem. Phys. **128**, 014303 (2008).
  - [55] B. Kendrick and R. T Pack, J. Chem. Phys. **102**, 1994 (1995).
  - [56] B. Kendrick, R. T Pack, J. Chem. Phys. **106**, 3519 (1996).
  - [57] C. Xu, D. Xie, D. H. Zhang, S. Y. Lin, and H. Guo, J. Chem. Phys. **122**, 244305 (2005).
  - [58] D. Xie, C. Xu, T.-S. Ho, H. Rabitz, G. Lendway, S. Y. Lin, and H. Guo, J. Chem. Phys. **126**, 074315 (2007).
  - [59] D. Quan, E. Herbst, T. J. Millar, George E. Hassel, S. Y. Lin, H. Guo, P. Honvault, and D. Xie, ApJ **681**, 1318 (2008).
  - [60] R. T Pack and G. A. Parker, J. Chem. Phys. **87**, 3888 (1987).
  - [61] B. K. Kendrick, R. T Pack, R. B. Walker, and E. F. Hayes, J. Chem. Phys. **110**, 6673 (1999).
  - [62] B. R. Johnson, J. Comp. Phys. **13**, 445 (1973).
  - [63] H. A. Bethe, Phys. Rev. **47**, 747 (1935).
  - [64] E. P. Wigner, Phys. Rev. **73**, 1002 (1948).
  - [65] In our previous study [33] we also used  $\rho_m = 44.0 \text{ a}_0$  for collision energies  $E_c < 10^{-4} \text{ eV}$ .
  - [66] D. C. Clary and H.-J. Werner, Chem. Phys. Lett. **112**, 346 (1984).
  - [67] J. M. Bowman, J. Phys. Chem. **95**, 4960 (1991).
  - [68] T. C. Germann and W. H. Miller, J. Phys. Chem. A **101**, 6358 (1997).
  - [69] D. E. Skinner, T. C. Germann, and W. H. Miller, J. Phys. Chem. A **102**, 3828 (1998).
  - [70] A. Viel, C. Leforestier, and W. H. Miller, J. Chem. Phys. **108**, 3489 (1998).
  - [71] M. M. Graff and A. F. Wagner, J. Chem. Phys. **92**, 2423 (1990).
  - [72] P. Langevin, Ann. Chim. Phys. **5**, 245 (1905).
  - [73] D. C. Clary, Mol. Phys. **53**, 3 (1984).
  - [74] J. Davidsson and G. Nyman, Chem. Phys. **125**, 171 (1988).
  - [75] M. T. Cvitaš, P. Soldán, J. M. Hutson, Mol. Phys. **104**, 23 (2006).
  - [76] M. Rerat, B. Bussery-Honvault, Mol. Phys. **101**, 373 (2003).